J. Fluid Mech. (1972), *vol.* 56, *part* 4, *pp.* 695–719
Printed in Great Britain

Experiments on the nonlinear stages of free-shear-layer transition

By RICHARD W. MIKSAD

Department of Meteorology, Massachusetts Institute of Technology†

(Received 2 November 1971 and in revised form 3 May 1972)

An experimental study is made of the instability and transition of a laminar free shear layer by sound excitation. Primary emphasis is placed on the nonlinear stages of transition. Transition from laminar instability to turbulent breakdown covers approximately five wavelengths of downstream distance. The instability has six distinct regions of behaviour: a region of exponential growth described by linear theory; a nonlinear region where critical-layer effects are important, and harmonics and subharmonics are generated; a region of finite amplitude equilibration of the fundamental mode; a region of finite amplitude triggered subharmonic instabilities; a region of three-dimensional longitudinal vortex formation; and a final region of weak secondary instabilities and turbulent breakdown.

1. Introduction

Free-shear-layer instability and transition occur randomly in fully turbulent flow; such phenomena must play an important part in the process of generation and maintenance of turbulence. The present experiments on instability and transition in a free shear layer may help our understanding of some of the more complicated processes which occur in turbulent flow; the results may form the basis for further analysis.

Our work builds upon the previous work of Sato (1956, 1959, 1960), Sato & Kuriki (1961), Sato & Okada (1966), Browand (1966) and Freymuth (1966). Their work established the applicability of linear theory to the early stages of instability, and the presence of subharmonic oscillations and weak secondary instabilities. Kelly (1967) obtained analytical explanations for the subharmonic oscillation. Landau (1944), Stuart (1960) and Watson (1960) have studied finite amplitude effects on disturbance growth. The present results in general support their theoretical results and present a more detailed picture of the sequence of instabilities and interactions which lead to transition.

† Present address: Division of Atmospheric Sciences, University of Miami, Coral Gables, Florida.

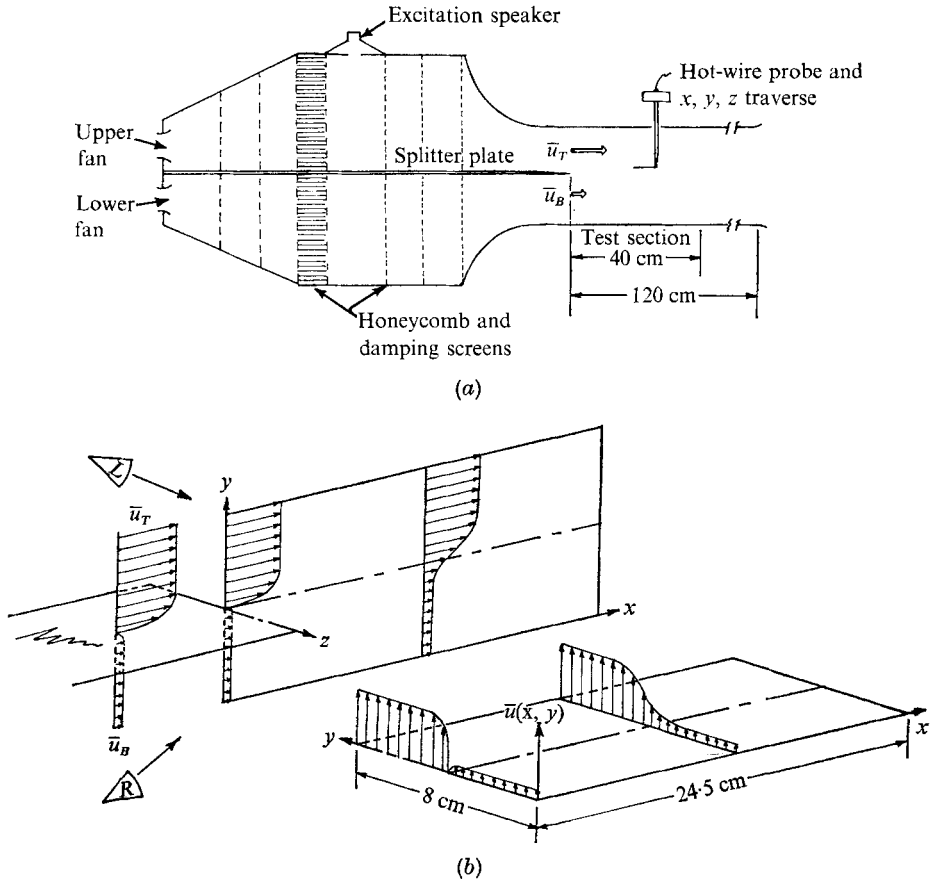

FIGURE 1. (*a*) Schematic drawing of the experimental apparatus, not to scale. (*b*) Co-ordinate reference frame for the data plots in figures 2 and 3. Figures 4 and 5 use the same format. Viewing angles L and R are for the left- and right-hand plots in figure 9. Figure 5 is viewed from L.

2. Experimental arrangement

The small low turbulence tunnel built for the experiment is shown in figure 1 (*a*), while figure 1 (*b*) shows the co-ordinate system. The test section, where the two streams join to form the free shear layer, is 12·5 × 13·5 cm in cross-section and 40 cm long. The angle between the side walls was adjusted to give zero streamwise pressure gradient for the first 25 cm downstream of the splitter plate. An automatic traversing mechanism allowed the position of a hot-wire anemometer (Shapiro & Edwards Model 50, constant current) to be programmed in a continuous traverse in any direction. Most of the results presented in this paper were obtained by traversing the hot wire at a low speed normal to the mean stream at streamwise locations 0.5 cm apart for fifty downstream locations. The mean and fluctuating components of probe signal, as well as the excitation signal and voltages corresponding to x, y, z probe position were simultaneously recorded on separate tracks of a magnetic tape for later analog and digital

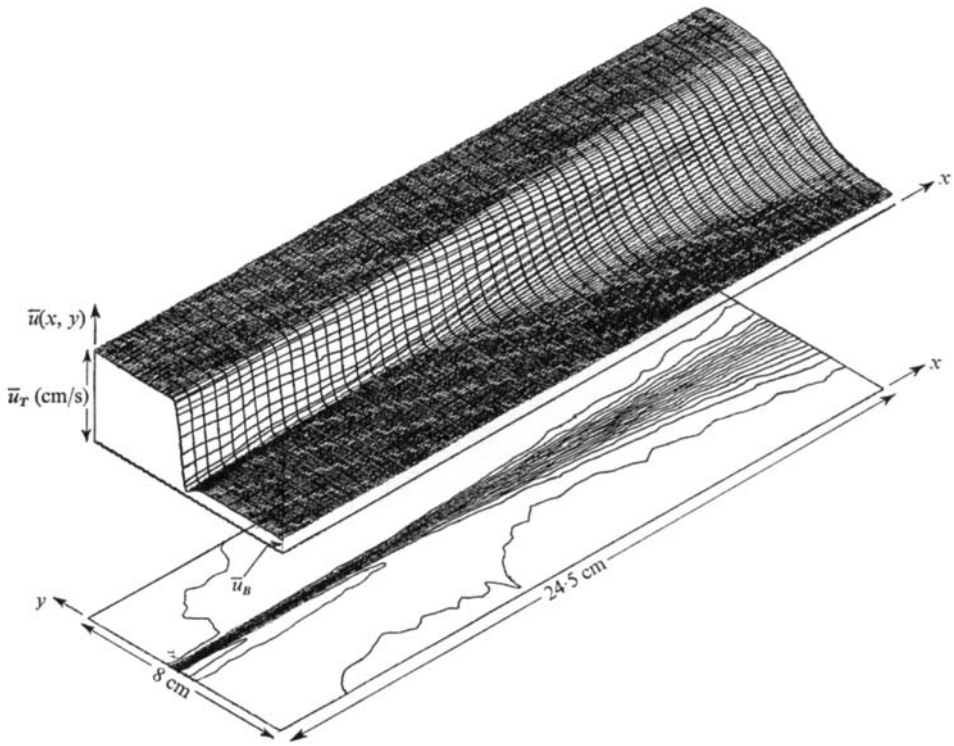

FIGURE 2. Vertical profiles of mean velocity $\bar{u}(x, y)$ and contours of constant velocity in naturally excited instability. Velocity profiles made at 0·5 cm downstream intervals. Contour interval is $\bar{u}/\bar{u}_T = 0{\cdot}05$. $\bar{u}_T = 203$ cm/s, $\bar{u}_B = 33$ cm/s, Reynolds number = $[\Delta\bar{u}\theta_m(x_0)]/\nu = R(x_0) = 150$.

analysis. Each traverse gave the local vertical distribution of r.m.s. velocity of all frequency components in the instability. Since the results for a given set of parameters were obtained in a single set of runs, problems of repeatability of experimental conditions were largely eliminated.

The absolute error in mean flow velocity is of order 3 % with a relative accuracy of 1 %. The error in velocity fluctuations is estimated to be of order $\pm$ 5 %.

The choice of using two streams to generate the shear layer rather than using a flow into air at rest enabled us to have all fluctuations occurring as perturbations on a mean flow. This made hot-wire measurement much simpler as it minimized instrumentation problems encountered when signal amplitudes are large compared with local mean velocity. A second advantage in using merging streams is that the velocity of propagation of disturbances was increased by advection, making spatial growth rates less than that for a shear flow into a medium at rest. This gave better spatial resolution, although we did not find it necessary to take full advantage of this feature.

3. The mean velocity field

Figure 2 shows the mean velocity as a function of x (to the right) and y (back to the left), where x is downstream and y is normal to the splitter plate. On a

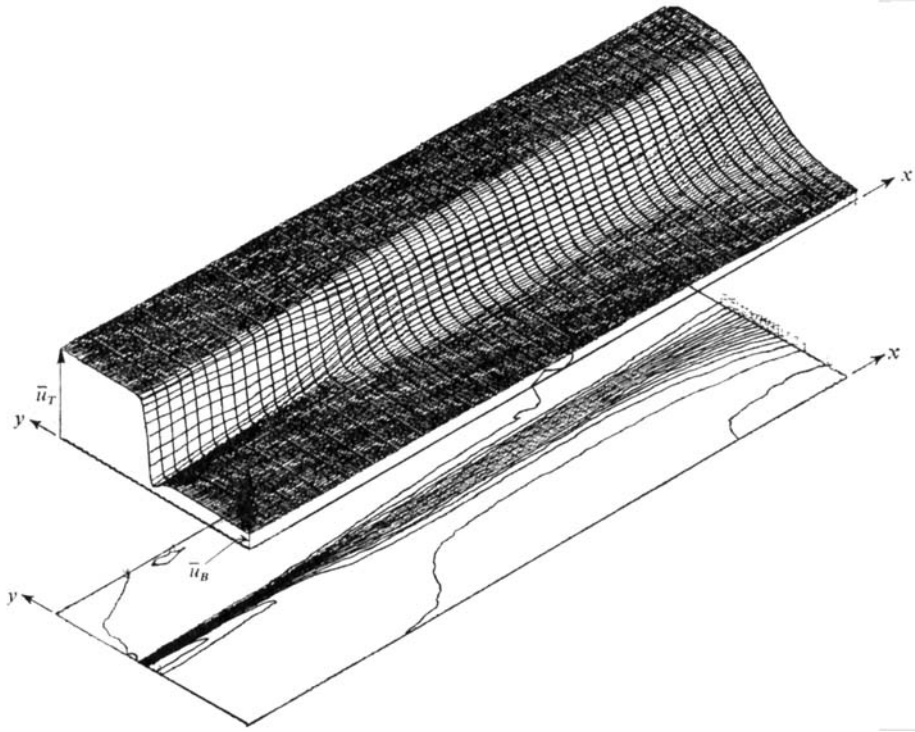

FIGURE 3. Vertical profiles of mean velocity $\bar{u}(x, y)$ and contours of constant velocity when $\beta = 0{\cdot}222$ is excited. $\beta = 0{\cdot}222$ is near most unstable disturbance. Contour interval is $\bar{u}/\bar{u}_T = 0{\cdot}05$. $\bar{u}_T = 202$ cm/s, $\bar{u}_B = 38$ cm/s, $R(x_0) = 145$.

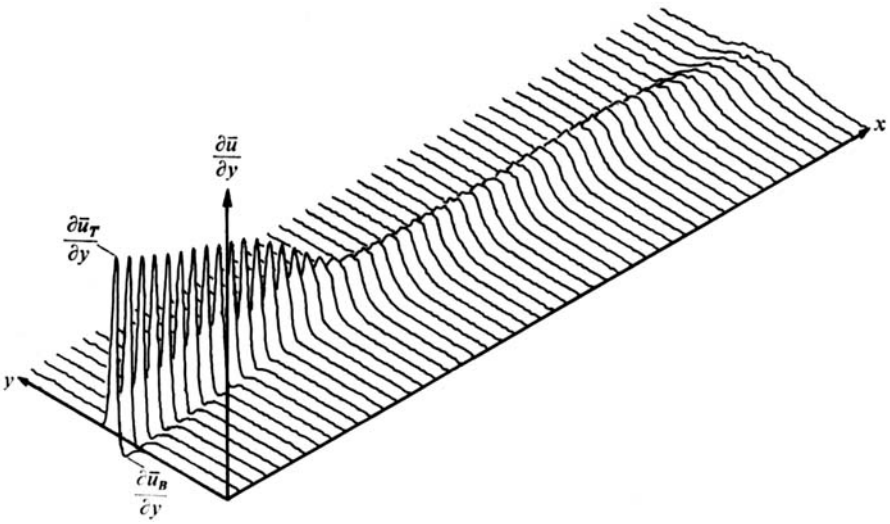

FIGURE 4. Vertical profiles of mean vertical shear $\partial\bar{u}/\partial y$. $\beta = 0{\cdot}222$ is excited. Profiles made at 0·5 cm downstream intervals. $(\partial\bar{u}/\partial y)_T = 641$ s^{-1}, $(\partial\bar{u}/\partial y)_B = -62$ s^{-1}, $R(x_0) = 145$.

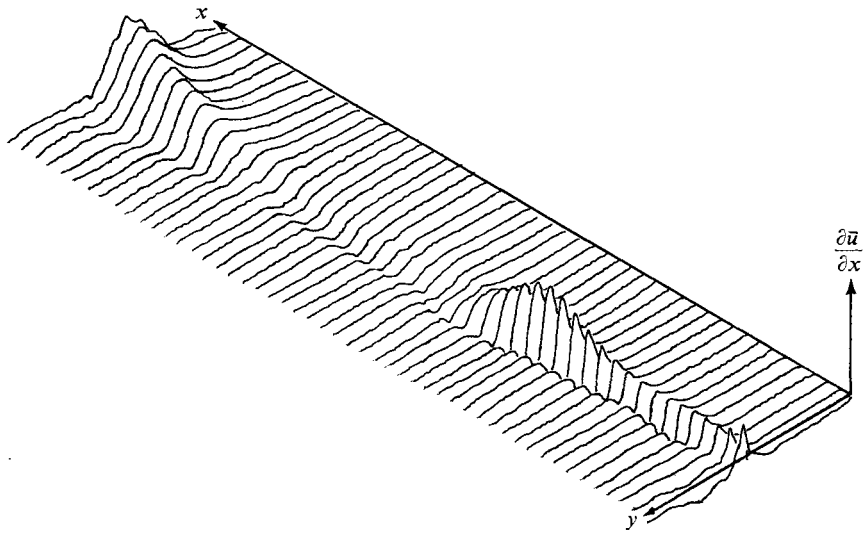

FIGURE 5. Vertical profiles of mean downstream shear $\partial\bar{u}/\partial x$. $\beta = 0{\cdot}222$ is excited. Profiles made at 0·5 cm downstream intervals. $(\partial\bar{u}/\partial x)_{\max} = 13\ \mathrm{s}^{-1}$ at x_0, $R(x_0) = 145$.

plane below are projections of the contours of constant velocity. This mean velocity field was measured with natural instability and transition in the shear layer. It is strongly two-dimensional in the central 8×8 cm of the test section. Note the wake of the plate and the almost parallel flow region which persists for approximately ten shear-layer thicknesses. For contrast, figure 3 shows the mean velocity field during artificial excitation of the most unstable mode of instability. Note how there are now two regions of almost parallel flow. This latter feature is also apparent in the profiles of vertical shear $\partial\bar{u}/\partial y$ shown in figure 4, while the downstream variations of $\partial\bar{u}/\partial x$ shown in figure 5 provide a measure of the departure from parallel flow. Having established some of the features of the mean flow, we now proceed to show the results for natural and forced instability and transition.

4. Instability and transition

The Reynolds numbers of the two boundary layers on the splitter plate were both below the critical Reynolds number for laminar boundary-layer instability. Growing disturbances in the wake of the splitter plate must therefore be caused by instability of the free shear layer.

The field of velocity fluctuations will be described as a sum of terms of the form

$$u'(\mathbf{x}, t) = 2^{\frac{1}{2}} u'_{\mathrm{r.m.s.}}(\mathbf{x}) \exp\left[i(\alpha_r x - \beta t + \phi_2 + \phi_3) - \alpha_i x\right],$$

where α_r and β are downstream wavenumber and frequency. ϕ_2 and ϕ_3 are phase angle variations with y and z (where z is parallel to the mean vorticity) and $-\alpha_i$ is the spatial growth rate in the downstream x direction.

Natural instability and transition

The results for disturbances excited by the free-stream turbulence and extraneous noise are shown for reference in figure 6, which contains a set of spectra of streamwise velocity fluctuations measured at $y = 0{\cdot}2$ cm for a number of downstream positions. The spectra show first a maximum near 16 Hz and, further downstream, a maximum near 8 Hz. This is in agreement with previous observations of Browand (1966) and others.

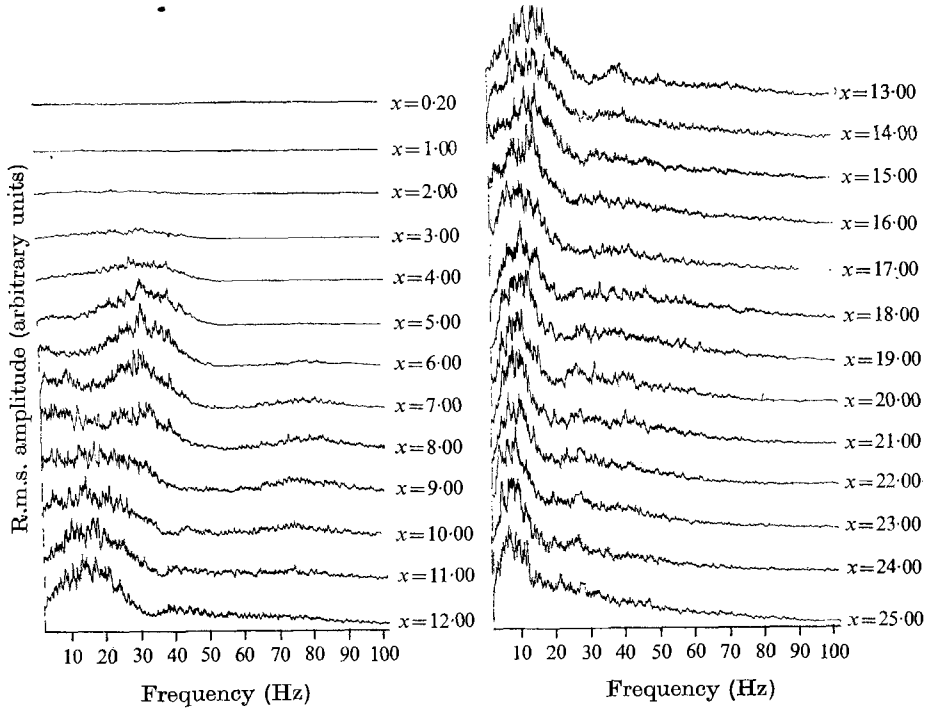

FIGURE 6. Downstream frequency spectra of disturbances in natural excited instability. $y = 0{\cdot}2$ cm, bandwidth = 1·0 Hz, sweep speed = 0·055 Hz/s, time constant = 10 s. $\overline{u}_T = 230$ cm/s, $\overline{u}_B = 38$ cm/s, $R(x_0) = 170$. x is measured in centimetres.

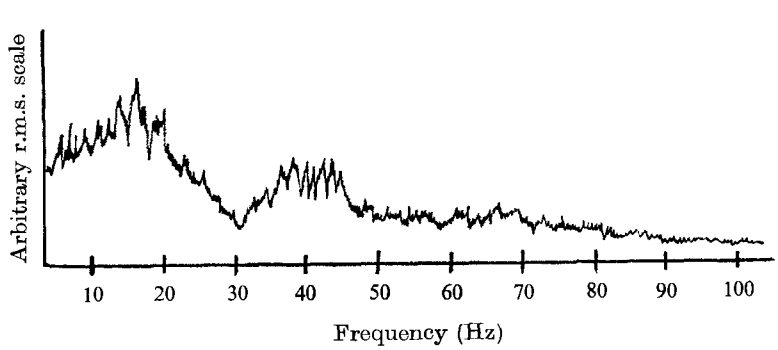

FIGURE 7. Frequency spectra in natural excited instability. $x = 12{\cdot}00$ cm, $y = 0{\cdot}0$ cm, amplitude axis is in arbitrary units, bandwidth = 1·0 Hz, sweep speed = 0·055 Hz/s, time constant = 10 s, $R(x_0) = 170$.

Oscillations at 16 Hz and 45 Hz, the sub- and $\frac{3}{2}$-harmonic frequencies of the dominant fundamental, were evident in spectra taken at other vertical locations. A sample is shown in figure 7. The presence of subharmonic oscillations is a definite feature of free-shear-layer instability and is not due to nonlinear instrument response. Sub- and $\frac{3}{2}$-harmonics did not appear when the mean flow was changed to a symmetric wake. This is in agreement with the previous observations of Sato & Okada (1966).

The spectra in figures 6 and 7 were made with a Quan Tech 304 Spectrum Analyser, using a bandwidth of 1·0 Hz at 3 dB down (maximally flat Butterworth type with 24 dB slopes) and a sweep of 0·055 Hz/s, with a 10 s time constant.

Methods of excitation of disturbances

Regular sinusoidal disturbances were introduced by means of a loudspeaker placed in the upper stagnation chamber. The frequency of excitation was much lower than the frequency of sound waves of wavelengths comparable to the dimensions of the apparatus. The turbulence level in the tunnel was 10^{-4} times $\bar{u}_T$, the velocity of the upper stream. The loudspeaker injected a disturbance flow field of order 10^{-3} r.m.s.; typical r.m.s. amplitudes of the excited instability fluctuations were of order 10^{-2} r.m.s. The r.m.s. velocities given in this paper are all normalized with $\bar{u}_T$, the velocity of the upper stream.

It is believed that the principal effect of the loudspeaker excitation was to shift the location of the stagnation point on the splitter plate up and down, thus injecting vorticity in the free shear layer. This supposition is supported by our observation that a loudspeaker placed at the downstream end of the wind tunnel was rather ineffective in exciting shear-layer disturbances and, in particular, antisymmetric disturbances.

5. Experimental results

A number of naturally unstable modes were excited and their instability studied. Details of the instabilities depend on excitation frequency, but their overall features are qualitatively similar. Attention will be focused on the instability excited at 29·5 Hz, which is near the frequency of the most unstable disturbance of the natural transition.

Figure 8 shows frequency spectra of streamwise velocity fluctuations for different values of x at $y = 0{\cdot}2$ cm, using an excitation frequency of 29·5 Hz (i.e. $\beta = 0{\cdot}222$). It is evident that the disturbance field is much more organized in terms of discrete frequency components than is the case for natural instability. The generation of sharply centred harmonic modes is evident at $x = 5{\cdot}00$ cm. A broad shifting band of subharmonics centred at 16 Hz emerges at $x = 13{\cdot}00$ cm, while a similar shifting band of $\frac{3}{2}$-harmonics centred near 45 Hz appear slightly later. The downstream development of the vertical profiles of streamwise r.m.s. fluctuations is shown in figure 9. The profiles were made by traversing the shear layer at very low speeds (0·25 mm/s) as described earlier and passing the recorded signal through a band-pass filter. A bandwidth of $\pm$ 0·5 Hz was used for the

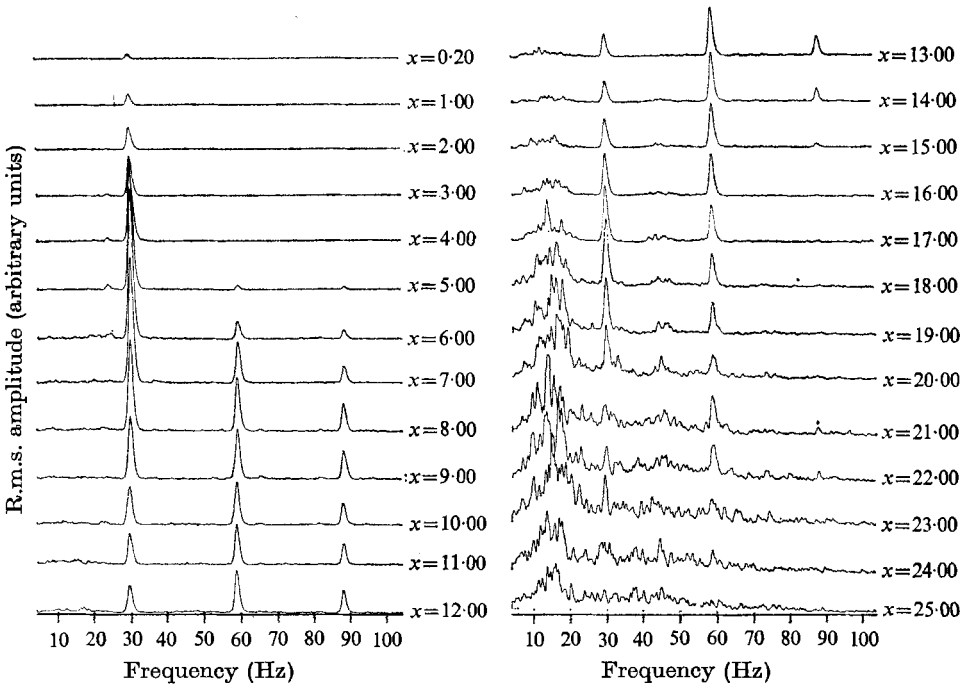

FIGURE 8. Downstream $u'_{\text{r.m.s.}}$ frequency spectra of disturbances. $\beta = 0{\cdot}222$ is excited. $y = 0{\cdot}2$ cm, bandwidth = 1·0 Hz, sweep speed = 0·55 Hz/s, time constant = 1 s, $\bar{u}_T = 210$ cm/s, $\bar{u}_B = 38$ cm/s, $R(x_0) = 152$.

harmonic modes, while a ± 5 Hz bandwidth was required for the broader sub- and $\frac{3}{2}$-harmonic bands.

Six distinct regions of downstream instability development were observed for the excited disturbances. For convenience they are referred to as regions I–VI and are identified in table 1 for the instability of the most unstable disturbance. The behaviour of other less unstable disturbances of higher and lower frequency will be noted where appropriate.

Region I: *initial instability and small amplitude growth*

In the initial small-amplitude region of transition, excited disturbances grow exponentially with downstream distance. The spatial growth rates of disturbances were determined two ways; in terms of the growth of the maximum amplitude of $u'_{\text{r.m.s.}}$, which grows as $\exp(-\alpha_i, x)$ and also in terms of E_u, which grows as $\exp(-2\alpha_i x)$, where

$$E_u(\beta, x) = \int_{-L}^{+L} \frac{u'^2_{\text{r.m.s.}}(\beta, x, y)}{2\theta_m(x_0)\bar{u}_T^2}\, dy.$$

L is much larger than the shear-layer thickness, and $\theta_m(x_0)$ is the sum of the momentum thickness of the two entering boundary layers. $\bar{u}_T$ is the maximum mean velocity of the upper stream. The measured growth rates are compared in figure 12 with spatial and temporal stability calculations based on the initial velocity field at x_0, the point of merging. The measured mean velocity

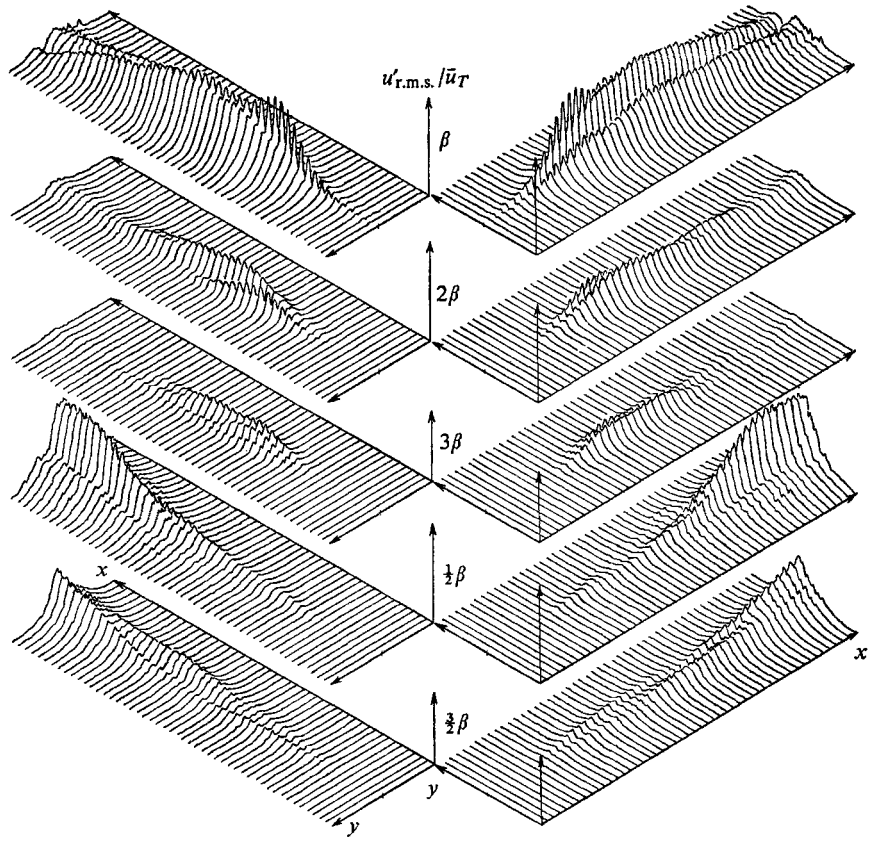

FIGURE 9. Vertical profiles of $u'_{\text{r.m.s.}}$ for disturbances in the spectra of the $\beta = 0{\cdot}222$ excited instability. Profiles made at 0·5 cm downstream intervals. $R(x_0) = 145$. β = fundamental mode, $u'_{\text{r.m.s.}}/\bar{u}_T$ amplitude axis = 0·155 full scale; 2β = second harmonic, amplitude axis = 0·155; 3β = third harmonic, amplitude axis = 0·055; $\frac{1}{2}\beta$ = subharmonic, amplitude axis = 0·155; $\frac{3}{2}\beta$ = $\frac{3}{2}$-harmonic, amplitude axis = 0·055.

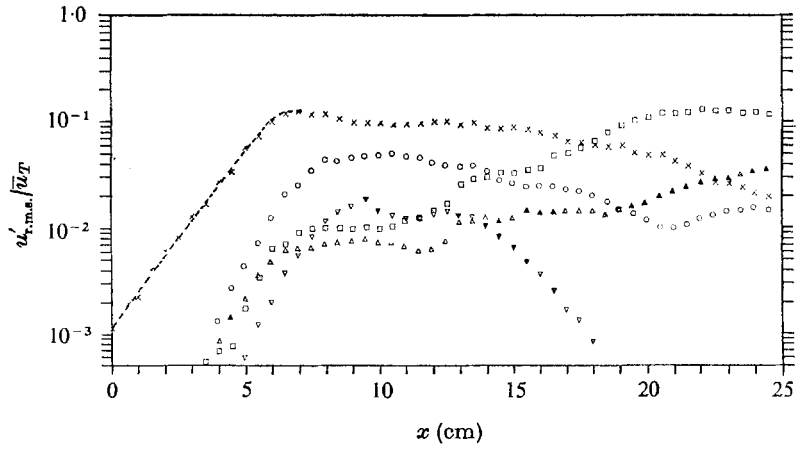

FIGURE 10. Downstream growth of $u'_{\text{r.m.s.}}$ maxima. Excitation at $\beta = 0{\cdot}222$; $R(x_0) = 145$. ×, β; ○, 2β; ▽, 3β; □, $\frac{1}{2}\beta$; △, $\frac{3}{2}\beta$. – – –, theoretical Landau equilibration curve.

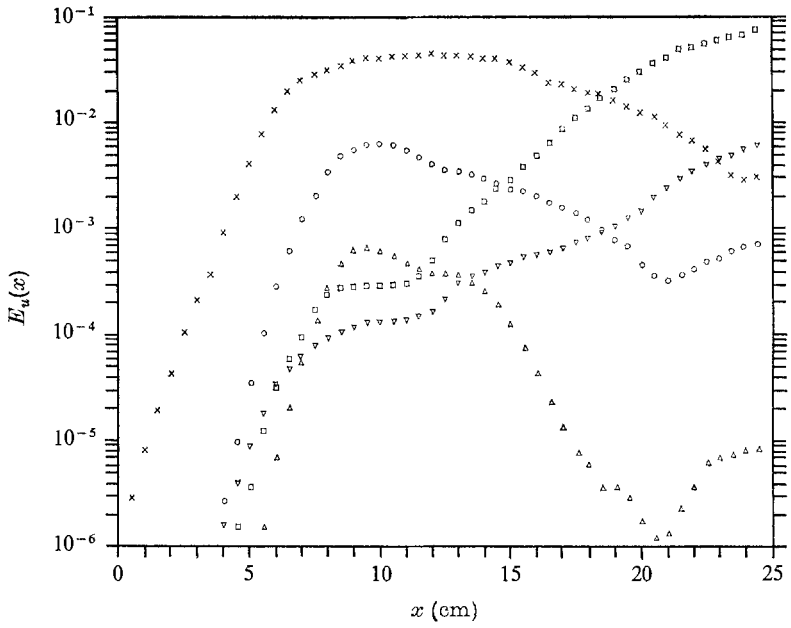

FIGURE 11. Downstream growth of E_u, the vertically integrated $u'_{\text{r.m.s.}}$ energy of disturbances when $\beta = 0{\cdot}222$ is excited; $R(x_0) = 145$. ×, β; ○, 2β; △, 3β; □, $\frac{1}{2}\beta$; ▽, $\frac{3}{2}\beta$.

Region	Approximate extent (cm)	Characteristics
I	0–3·50	Fundamental mode grows exponentially and obeys linear theory. No nonlinear modes are measurably present.
II	3·50–5·00	Fundamental mode continues to grow exponentially; harmonics and subharmonics appear, and grow exponentially. The harmonic modes are not unstable modes of the basic flow.
III	5·00–11·50	Fundamental mode deviates from exponential growth and equilibrates into finite amplitude oscillations; harmonics and subharmonics equilibrate in unison with the fundamental mode.
IV	11.50–14·00	Sub- and $\frac{3}{2}$-harmonics start a second region of growth; fundamental mode remains in equilibration; second and third harmonics start to decay.
V	14·00–20·50	Termination of fundamental mode equilibration. Three-dimensional distortions of the fundamental appear and a secondary vortex structure is formed; second and third harmonics decay strongly; sub- and $\frac{3}{2}$-harmonic growth rates decrease.
VI	20·50–24·50	Final breakdown into turbulence. Intermittent secondary instabilities appear; disturbance spectra loses discrete character. Three-dimensional activity dominates the flow.

TABLE 1. Identification of downstream characteristics of the instability excited at $\beta = 0{\cdot}222$. $R(x_0) = 150$, $\beta = (2\pi f \times 2\theta_m(x_0))/\overline{u}_T$.

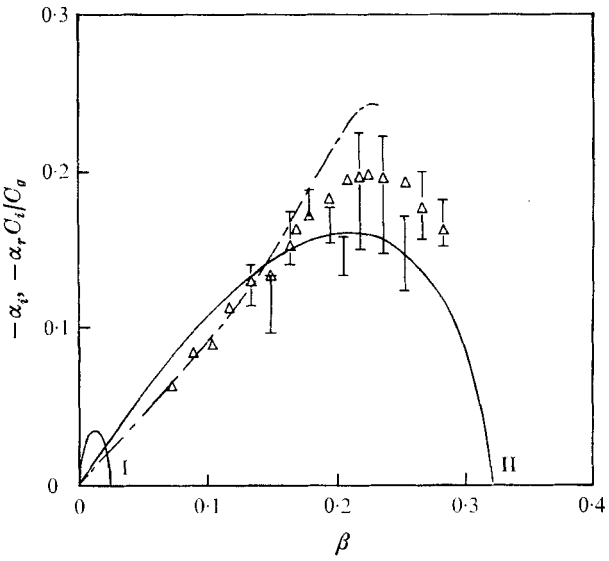

FIGURE 12. Spatial growth rates ($-\alpha_i$) of the unstable fundamental modes in the linear region of transition. △, experimentally measured growth rates of excited disturbances. Bars indicate spread in growth rates measured in the natural instability. – – –, $-\alpha_i$, theoretical spatial growth rates; ——, $-\alpha_r C_i/C_g$, theoretical temporal calculation growth rates. Theoretical calculations based on measured mean velocity profile at x_0.

profile was approximated by a trapezoidal profile (Howard 1964) and has two classes of instability: class I, due to the lower inflexion point, and class II, due to the upper inflexion point. The class I instabilities are of extremely low frequency and have small growth rates and long wavelengths. They could not be detected in the existing apparatus. The class II instabilities dominate the transition and are similar to the instabilities calculated by Michalke (1965) for a hyperbolic-tangent profile. The dominance of the class II modes reflects the difference in the maximum shears of the two entering layers.

Although maximum growth rates predicted by the two models differ by 34 %, the most unstable mode frequencies differ by only 5·8 % and are both centred near the frequency of the experimentally determined, most unstable mode. The neutral points of both models coincide and agree within experimental error with the neutral point observed in the natural transition. The difference in maximum growth rates predicted by the temporal and spatial models may be due to the fact that group velocity transformations are only valid for weakly amplified disturbances. This has also been noticed in experiments by Mattingly (1968).

The spatial calculations did not converge for large $|\alpha_r|$ and results are shown only up to the most unstable mode. The results of both models are given in table 2 along with the corresponding experimental values. The results of previous workers are included for comparison. These were typically obtained for single-inflexion-point shear layers and correspond to our class II instabilities; they have been scaled accordingly.

Experimental values of growth rate and phase speed were measured over the first wavelength of transition. In this distance, significant variations in

Model	Frequency (β)	Growth rate ($-\alpha_i$)	Wavenumber (α_r)	Phase speed (C_p)
Miksad (experiment)	0·2175	$-\alpha_i = 0{\cdot}1970$	0·380	0·570
Miksad (spatial)	0·2216	$-\alpha_i = 0{\cdot}2370$	0·414	0·536
Miksad (temporal)	0·2090	$\alpha_r c_i/c_p = 0{\cdot}1560$ $\alpha_r c_i/c_g = 0{\cdot}1540$	0·396	0·547
Browand (experiment)	0·227	$-\alpha_i = 0{\cdot}220$	$0{\cdot}36 \pm 0{\cdot}08$	$0{\cdot}58 \pm 0{\cdot}11$
Sato (experiment)	0·2208	$-\alpha_i = 0{\cdot}184$	0·37	$0{\cdot}54 \pm 0{\cdot}08$
Freymuth (experiment)	0·2140	$-\alpha_i = 0{\cdot}180$	—	—
Michalke (spatial)	0·2067	$-\alpha_i = 0{\cdot}2284$	0·4031	0·5137
Michalke (temporal)	0·223	$\alpha_r c_i/c_p = 0{\cdot}1898$	0·4446	0·5000

TABLE 2. Experimental and theoretical eigenvalues for the maximally unstable disturbance

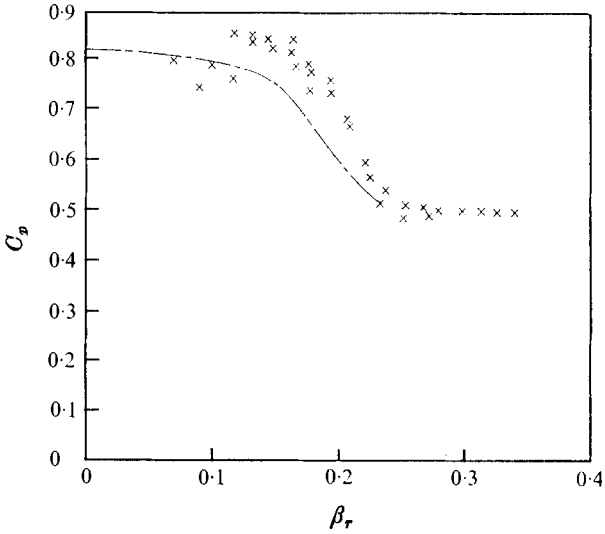

FIGURE 13. Measured values of phase speed C_p for excited disturbances. Measurements made in first 6·0 cm of growth. $R(x_0) = 160 \pm 20$. Dashed curve is the phase speed predicted by spatial stability calculations at x_0.

mean flow and maximum shear occur. The reasonably close agreement of growth rates and phase speeds with the theoretical results predicted for the initial velocity field at x_0 indicates an initial insensitivity of the instabilities to the evolving mean flow. The spreading of the mean flow only seemed to cause a downstream spreading in the disturbance $u'_{\text{r.m.s.}}$ profiles.

An interesting feature of the small-amplitude region is evident in figure 14, where variations in group velocity with frequency are plotted. The results show that the minimum group velocity occurred at the frequency of the most unstable mode.

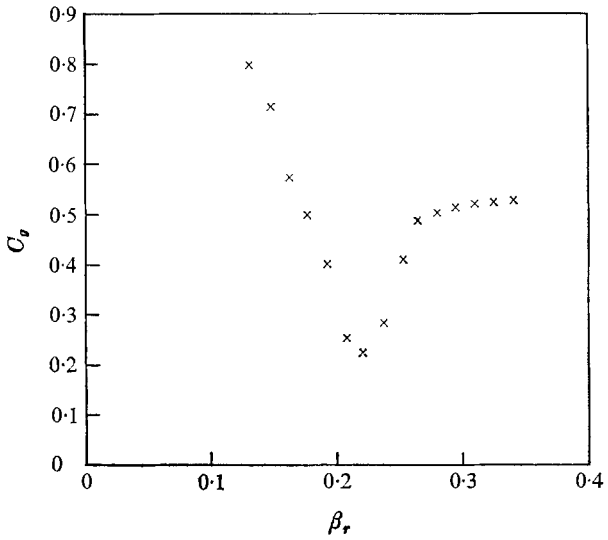

FIGURE 14. Experimentally computed group velocities C_g of the excited disturbances. Values calculated from a least-squares polynomial approximation to measured values of wavenumber and frequency.

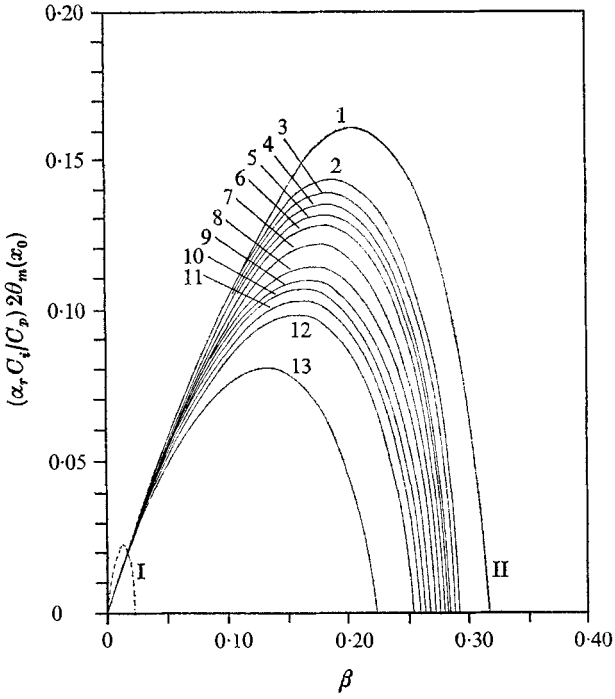

FIGURE 15. Downstream variations in disturbance growth rate predicted by temporal parallel-flow stability calculations based on locally measured mean velocity profiles. Dashed curve is the mode I instability at x_0. All other curves are for mode II instabilities.

Curve no.	1	2	3	4	5	6	7	8	9	10	11	12	13
x (cm)	x_0	0·5	1·0	1·5	2·0	2·5	3·0	3·5	4·0	4·5	5·0	5·5	6·0

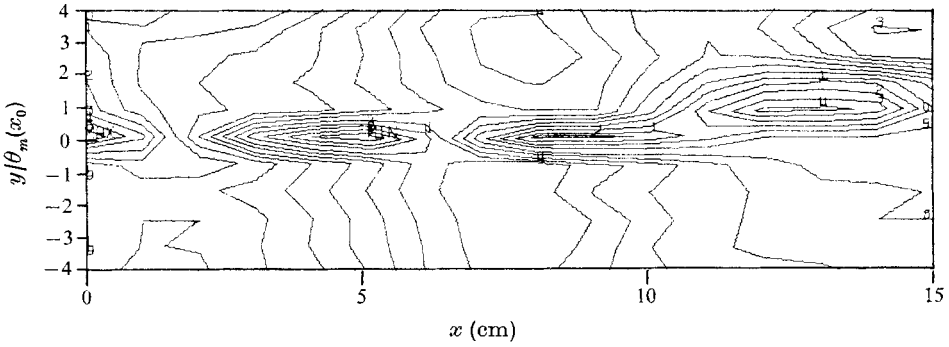

FIGURE 16. Contours of the downstream variations in 2π phase repetition distance for the $\beta = 0{\cdot}222$ disturbance as seen in a co-ordinate frame moving with the phase velocity of the fundamental mode. $\bar{u}_T = 210$ cm/s, $\bar{u}_B = 38$ cm/s, $R(x_0) = 150$.

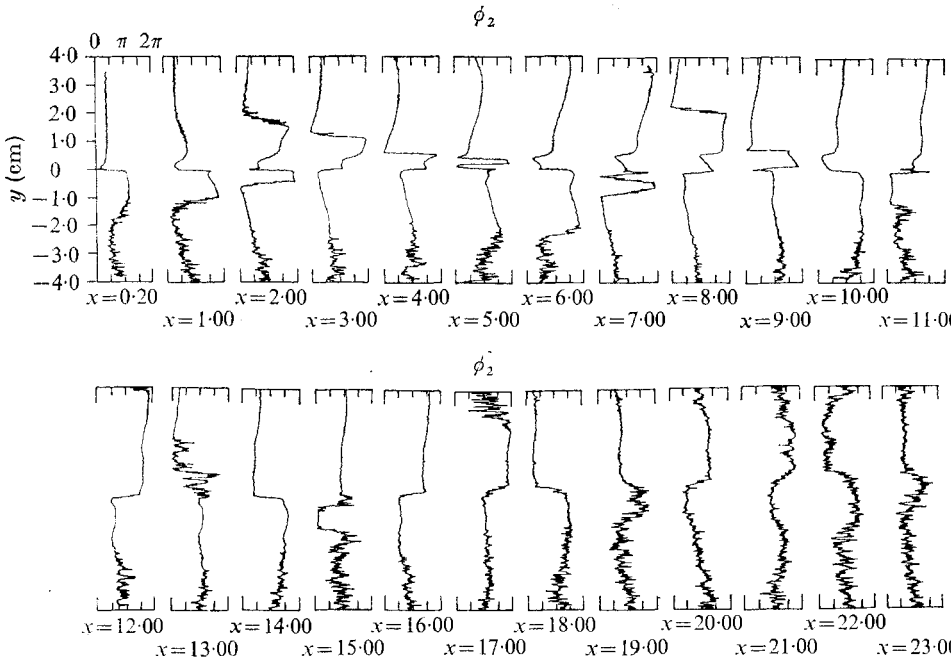

FIGURE 17. Downstream profiles of the vertical variations in phase of the $\beta = 0{\cdot}222$ disturbance. $R(x_0) = 150$. x measured in centimetres.

The stability characteristics of subsequent measured profiles beyond x_0 are shown in figure 15. Each succeeding profile was taken to represent a new parallel-flow stability problem. In each case a multi-sided trapezoidal velocity profile was fitted to the measured profiles. Because of poor spatial model convergence, temporal calculations were used as a rough estimate of downstream behaviour.

Disturbance wavelengths were measured by making downstream traverses and noting the distance between 2π changes in phase. Wavelengths measured on this basis showed considerable variation with vertical location. Similar results have been reported by Browand (1966) and others. Contours of 2π phase repetition

distance are plotted in figure 16. Miksad (1970) noted that the wavelength measuring technique used in this experiment, and by past workers, effectively transfers one's measurements to a co-ordinate frame moving with the disturbance phase velocity. The disturbance streamlines viewed in this frame form Kelvin's cat's eyes. We are not looking directly at disturbance streamlines in figure 16, but a similar structure is evident.

Although wavelengths measured by phase repetition varied with location, the characteristic streamwise scale of successive closed contours is relatively constant. For a simple travelling wave in a co-ordinate frame moving with the disturbance phase speed, the distance between the centres of successive streamline cat's eyes is equivalent to the disturbance wavelength. The distance between closed contours (as in figure 16) was used to evaluate some wavelengths in this experiment. Wavelengths measured by phase repetition tended to approach the cat's eye spacing as the outer edges of the shear layer were approached.

Phase variations in the vertical, shown in figure 17 for the 31 Hz disturbance, initially have a simple 180° change near the critical layer as predicted by linear spatial theory (Michalke 1965). However, the phase profiles evolve into a complicated structure as the disturbance amplitude increases. Spanwise phase measurements showed that the disturbance was two-dimensional in this region.

Region II: *onset of nonlinear activity*

Figure 10 shows that harmonic and subharmonic modes start to grow at $x = 4{\cdot}00$ cm. The fundamental mode amplitude is of order 2×10^{-2} times the $\overline{u}_T$. This is a smaller amplitude than that normally assumed for the onset of nonlinear activity and indicates a restriction on linear theory. The generation of harmonic modes coincides with a slight kink, at $x = 3{\cdot}50$ cm, in the E_u curve of the fundamental mode. This may represent a transfer of energy to the harmonic modes. Growth rates of the harmonics and subharmonics of four disturbances were measured and are given in table 3. The growth rates measured when $\beta = 0{\cdot}222$ and $\beta = 0{\cdot}162$ were excited are based on E_u growth. Those measured when $\beta = 0{\cdot}113$ and $\beta = 0{\cdot}264$ were excited are based on the growth of $u'_{\text{r.m.s.}}$ maxima and have a nominal scatter of ± 10 %.

Mode	$\beta = 0{\cdot}113$ $-\alpha_i$	$\beta = 0{\cdot}162$ $-\alpha_i$	$\beta = 0{\cdot}222$ $-\alpha_i$	$\beta = 0{\cdot}264$ $-\alpha_i$
β	0·110	0·138	0·197	0·180
2β	0·149	0·160	0·303	0·260
3β	0·169	0·230	0·302	0·282
4β	0·139	0·176	0·316	0·284
5β	0·163	0·187	0·290	0·313
$\frac{1}{2}\beta$	0·135	0·170	0·247	0·200
$\frac{3}{2}\beta$	0·186	0·164	0·187	0·183

TABLE 3. Measured spatial growth rates of disturbances when $\beta = 0{\cdot}113$, $0{\cdot}162$, $0{\cdot}222$ and $0{\cdot}262$ are excited respectively. $R(x) = 160 \pm 20$.

The measured growth rates of harmonic modes range from 1·15 to 1·73 times that of their fundamental. In particular all harmonics of $\beta = 0{\cdot}222$ grow nearly

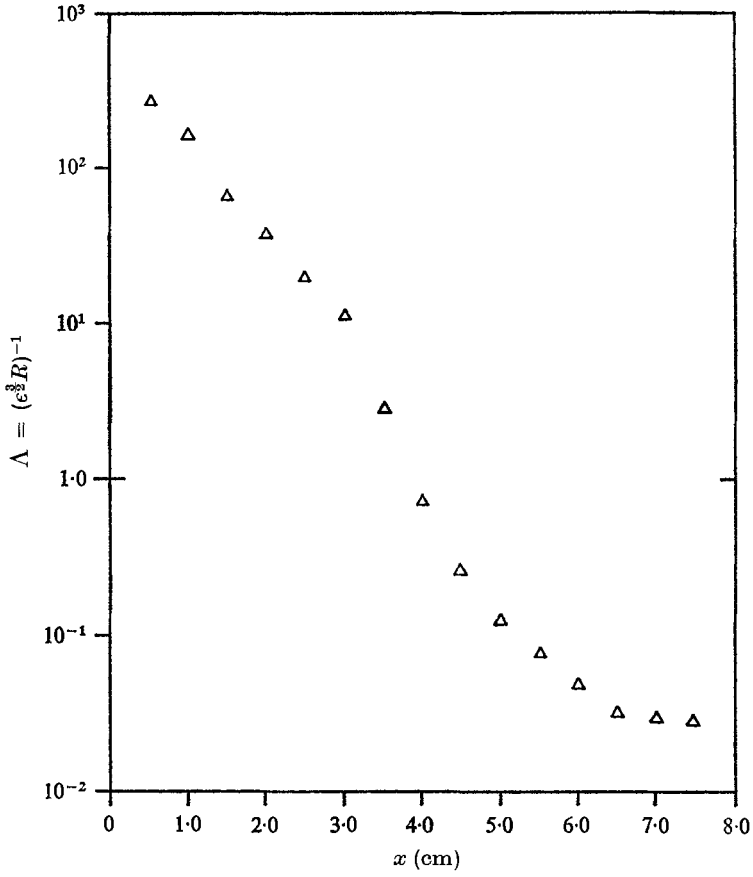

FIGURE 18. Downstream variations in $\Lambda = (\epsilon^{\frac{3}{2}}R)^{-1}$ when $\beta = 0{\cdot}222$ is excited. $R(x_0) = 150$.

1·5 times as fast as their fundamental. To within experimental accuracy, this holds for the harmonics of $\beta = 0{\cdot}264$. These are smaller growth rates than those predicted by weak nonlinear theories based on a viscous-dominated critical layer. However, as was pointed out by Dr J. Robinson (1971, unpublished manuscript), several features of harmonic growth agree with strong nonlinear theories which consider nonlinear terms at the critical layer.

The use of viscous terms leads to the traditional Orr–Sommerfeld problem with a viscous-dominated critical layer of order $\delta_v = |\alpha_r R|^{-\frac{1}{3}}$. Benney & Bergeron (1969) found that nonlinear terms give rise to a nonlinear-dominated critical layer of order $\delta_{nl} = \epsilon^{\frac{1}{2}}$, where ϵ is the disturbance amplitude. The appropriateness of the two approaches is determined by the parameter $\Lambda = (\epsilon^{\frac{3}{2}}R)^{-1}$, which can be viewed as proportional to $(\delta_v/\delta_{nl})^3$; R is the local Reynolds number. Viscous theory applies when $\Lambda \gg 1$, nonlinear theory when $\Lambda \ll 1$. At $\Lambda = O(1)$ both mechanisms must be considered. Note that even for moderate Reynolds numbers a large disturbance amplitude can make Λ approach $O(1)$.

Measured values of $\epsilon(x)$ and Reynolds number (based on local momentum thickness) were used to calculate $\Lambda(x)$. As is shown in figure 18, Λ approaches

$O(1)$ at the point where harmonics of $\beta = 0{\cdot}222$ are generated, indicating that nonlinear effects at the critical layer may be important.

Robinson found that, for $\Lambda \ll 1$, nonlinear effects in a free shear layer can force all harmonics at order ϵ or $\epsilon^{\frac{3}{2}}$, giving rise to harmonic growth rates of 1 or 1·5 times that of the fundamental. The order of forcing depends on the location of the critical point and mean flow inflexion point. If the two coincide, harmonics are forced at $\epsilon^{\frac{3}{2}}$. If the two are well separated, harmonics are forced at order ϵ. In the instabilities excited at $\beta = 0{\cdot}222$ and 0·264, the critical point and inflexion point almost coincide at $x = 4{\cdot}00$ cm, and measured harmonic growth rates are nearly 1·5 times that of their fundamental. The agreement with the theory is close, even though Λ is of order one. In the instabilities excited at $\beta = 0{\cdot}162$ and 0·113, the critical and inflexion points are separated, but the separations are of order δ_{nl}. The measured growth rates of the harmonics of $\beta = 0{\cdot}162$ and 0·113 roughly fall between 1 and 1·5 times that of their fundamentals.

First region of sub- and $\frac{3}{2}$-harmonic generation. The generation of harmonics at $x = 4{\cdot}00$ cm is accompanied by weak intermittent sub- and $\frac{3}{2}$-harmonic oscillations. The fundamental mode amplitude, of order 2×10^{-2} times the $\overline{u}_T$ velocity, is smaller than that reported by past workers for subharmonic activity. Browand (1966), for example, found sub- and $\frac{3}{2}$-harmonics only after the fundamental equilibrated at finite amplitudes of order 10^{-1} times the $\overline{u}_T$ velocity. The presence of small exponentially growing sub- and $\frac{3}{2}$-harmonic oscillations in this experiment is not felt to be spurious or due to nonlinear instrument response. Subharmonic oscillations were measured in regions of flow where disturbance amplitudes were small compared with the local mean velocity. Subharmonic oscillations did not appear in measurements of instability of symmetric wakes made with the same hot-wire system. The early growth of sub- and $\frac{3}{2}$-harmonic oscillations seems to be an inherent feature of the instability of separated free shear layers.

The growth rates of the sub- and $\frac{3}{2}$-harmonic modes are of the same order as the harmonic mode growth rates but it is not clear whether their generation is connected with the generation of harmonics. For example, although sub- and $\frac{3}{2}$-harmonics start to grow at the same location as the harmonics in the $\beta = 0{\cdot}222$ and $\beta = 0{\cdot}162$ instabilities, they are generated at earlier locations in the $\beta = 0{\cdot}113$ and $\beta = 0{\cdot}264$ instabilities. This was especially noticeable for $\beta = 0{\cdot}264$ excitation, where subharmonic oscillations appeared half a fundamental mode wavelength before the second harmonic.

Raetz (1959) considered interactions which can lead to the generation of difference frequency modes. Such an interaction between two growing fundamentals, one of which has half the frequency of the other, can produce a subharmonic. The growth rate of the generated mode is the sum of the rates for the two interacting modes. For $\beta = 0{\cdot}222$ and $\beta = 0{\cdot}162$ excitation, the measured subharmonic growth rates were close to the sum of the measured fundamental growth rate and the theoretical spatial growth rate of the half-frequency mode as calculated by linear theory at $x = 4{\cdot}00$ cm.

The measured relative rates of sub- and $\frac{3}{2}$-harmonic growth vary with excitation frequency. In low-frequency excitation, for $\beta < 0{\cdot}162$ the $\frac{3}{2}$-harmonic growth

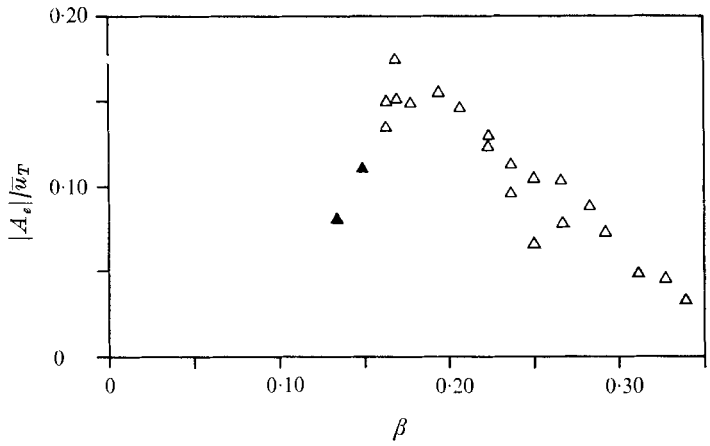

FIGURE 19. Equilibration amplitudes of excited disturbances. Solid symbols represent modes influenced by test section boundaries. $R(x_0) = 160 \pm 20$.

rate usually exceeds that of the subharmonic. For $\beta > 0{\cdot}162$ the subharmonic growth rate generally exceeds that of the $\frac{3}{2}$-harmonic. This may reflect the fact that for $\beta < 0{\cdot}162$ and sub- and $\frac{3}{2}$-harmonic frequencies are valid unstable modes of the basic flow (with the $\frac{3}{2}$-harmonic frequency more unstable). The opposite is true for $\beta > 0{\cdot}162$ where the $\frac{3}{2}$-harmonic is often a stable or nearly stable mode of the basic flow.

Region III: *finite amplitude equilibration*

At approximately $x = 5{\cdot}00$ cm the growth of the fundamental mode starts to deviate from its initial exponential rate (see figures 10 and 11). By $x = 7{\cdot}00$ cm the deviation is significant and by $x = 9{\cdot}00$ cm the r.m.s. amplitude and E_u energy equlibrate into relatively constant finite values. Equilibration persists until $x = 14{\cdot}00$ cm, when strong three-dimensional distortions occur. The problem of finite amplitude equilibration was first considered by Landau (1944), and later by Stuart (1960) and others. Liu (1969) considered the problem of spatially growing disturbances and showed that the amplitude of the equilibrating fundamental is governed by an equation of the form

$$d|\epsilon(x)|^2/dx = |\epsilon(x)|^2(2a_{0r} + 2a_{1r}|\epsilon(x)|^2), \tag{5.1}$$

where $\epsilon(x)$ is the fundamental mode amplitude and a_{1r} is the Landau coefficient. It represents the first-order and nonlinear dynamics which can act to limit fundamental mode growth. Equation (3.1) has the solution

$$|\epsilon(x)|^2 = a_{0r}Ce^{2a_{0r}x}/(1 - a_{1r}Ce^{2a_{0r}x}),$$

where C is an arbitrary real constant determined experimentally by the initial conditions at x_0.

In the limit of small amplitudes the disturbance growth must be exponential, and $a_{0r} = -\alpha_i$. If equilibration is to occur, a_{1r} must be non-zero, negative and equal to $A_e/-\alpha_i$ (where A_e is the equilibration amplitude). Measured values of A_e, $-\alpha_i$ and the initial amplitude were used to determine a_{1r} and C for the $\beta = 0{\cdot}222$ fundamental mode. $|\epsilon(x)|^2$ was then evaluated. As shown in figure 10, the

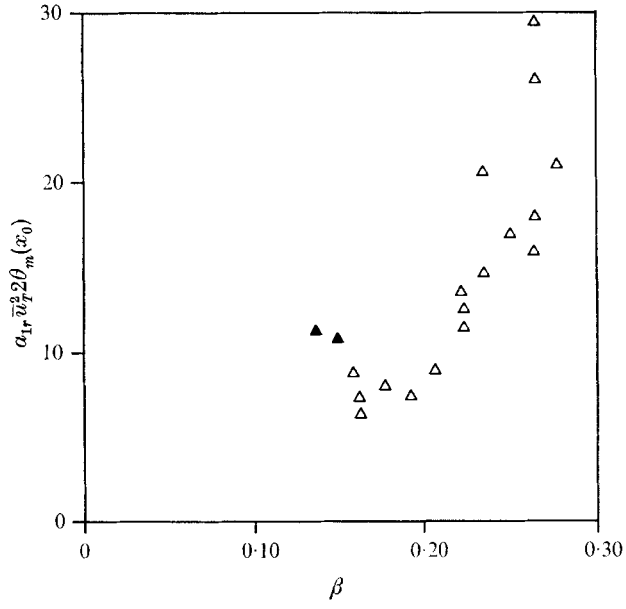

FIGURE 20. Values of Landau coefficients of excited disturbances. Solid symbols represent disturbances influenced by test section boundaries. $R(x_0) = 160 \pm 20$.

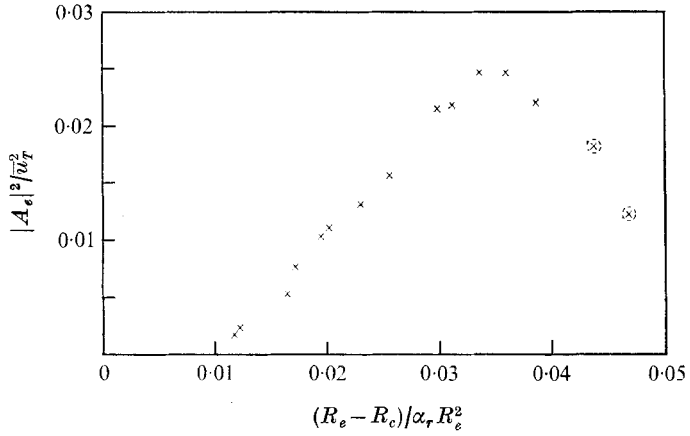

FIGURE 21. Dependence of equilibration amplitudes on local $(R_e - R_c/\alpha_r R_e^2)$ Reynolds number relation at equilibration. Circled modes are influenced by test section boundaries. $R(x_0) = 160 \pm 20$. Values of R_c from Betchov & Szewczyk (1963).

agreement with experiment is close. Values of a_{1r} were also determined for other fundamental modes and as shown in figure 20, a_{1r} tends to increase with frequency.

Stuart (1958), by making certain approximations, was able to show for a limited range of Reynolds numbers in plane Poiseuille flow that the equilibrium amplitude is determined by the Reynolds number at equilibration:

$$|A_e|^2 = [K_e(Re - R_c)]/\alpha_r R_e^2.$$

The coefficient K_e measures the ratio of net energy transfer to the fundamental (including viscous dissipation) to the rate at which Reynolds stress distortions of

the mean flow reduce its ability to transfer additional energy to the fundamental mode. If the two are in balance, $K_e = O(1)$.

Measured values of equilibration amplitudes and Reynolds numbers are shown in figure 21; the experimental points fall along a relatively straight line with unit slope (i.e. $K_e = O(1)$ for all modes except the long wavelength, low-frequency modes, which are influenced by the test section boundaries). The unit slope indicates that, to a good approximation, Stuart's approach may be applicable to free-shear-layer equilibration.

As is indicated in figures 19, 20 and 21, the small test section geometry exerted a limiting influence on the growth of long wavelength disturbances. Howard (1964) considered the influence of boundaries on temporally growing disturbances in a hyperbolic-tangent mean flow bounded by rigid walls at $\pm y_0$. His results indicate that the finite spacing of the boundaries will tend to stabilize disturbances for $\alpha_r y_0 \leqslant 1{\cdot}997$, which for the present test section geometry corresponds to $\alpha_r \leqslant 0{\cdot}20$. Boundary influence was experimentally observed for $\alpha_r < 0{\cdot}175$. Disturbances excited below this value initially grow at exponential rates predicted by linear theory, but equilibrate at smaller amplitudes than those reported by Freymuth (1966).

Region IV: *second region of subharmonic growth*

At $x = 10{\cdot}5$ cm, the sub- and $\frac{3}{2}$-harmonic modes undergo a strong but intermittent region of nearly exponential growth. The existence of a definite stop in sub- and $\frac{3}{2}$-harmonic growth between regions II and IV suggests that the responsible mechanisms differ in the two regions. As figures 10 and 11 show, the second region of subharmonic growth coincides with a definite equilibration of the fundamental at an amplitude of order 0·12 times the $\overline{u}_T$ velocity. This is equivalent to $u'_{\text{r.m.s.}}/\Delta\overline{u} = 0{\cdot}145$, where $\Delta\overline{u}$ is the velocity difference across the shear layer. The E_u energy of the fundamental mode is not affected by the onset of subharmonic growth. A similar result was noted by Browand (1966), and, as suggested by Kelly (1967), may indicate that the fundamental mode is acting as a catalyst to allow the direct passage of energy from the mean flow to the subharmonic.

Apart from the intermittency of the subharmonic, the essential features of this region are consistent with the work of Kelly (1967), which showed that finite amplitude oscillations of the fundamental can act to reinforce subharmonic oscillations without decreasing the energy of the fundamental itself. He found a critical threshold amplitude of $u'_{\text{r.m.s.}}/\Delta\overline{u} = 0{\cdot}12$. This is in reasonable agreement with the measured value of 0·145. The measured subharmonic growth rate is 0·093, roughly half that predicted by Kelly's analysis. This may be due to the fact that Kelly considered temporally growing disturbances, while the experimental disturbances are dispersive and grow spatially. The resonance matching conditions in Kelly's analysis are sensitive to dispersion.

Spanwise measurements of the fundamental mode showed it to be strongly two-dimensional at the point where subharmonic growth is triggered. No measurements of the spanwise structure of the subharmonic were made. The two-dimen-

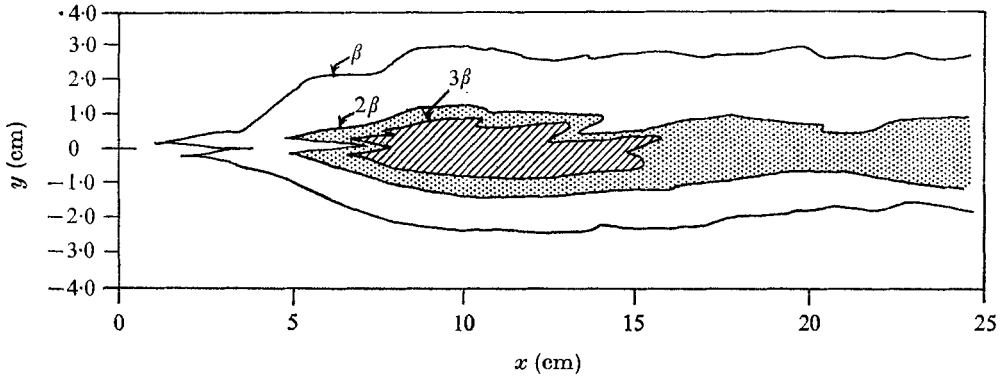

FIGURE 22. Contours of fundamental mode, second harmonic and third harmonic activity. Contours are for $u'_{\text{r.m.s.}}/\overline{u}_T$ equal to 0·005. $R(x_0) = 145$.

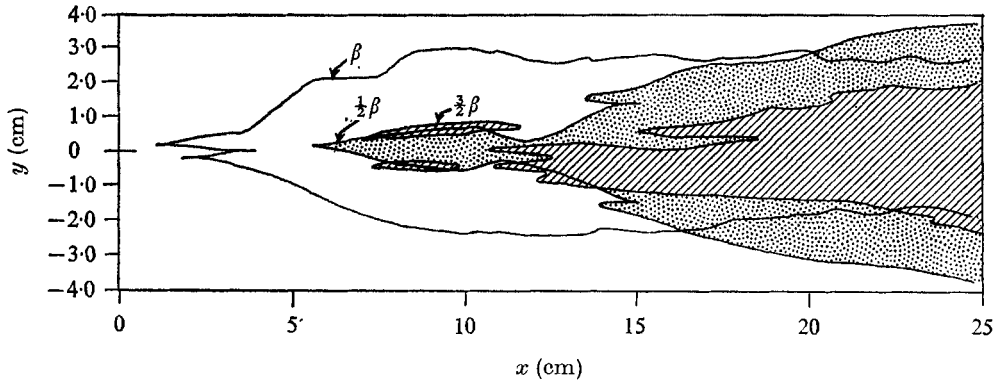

FIGURE 23. Contours of fundamental mode, subharmonic, and $\frac{3}{2}$-harmonic activity. Contours are for $u'_{\text{r.m.s.}}/\overline{u}_T$ equal to 0·005. $R(x_0) = 145$.

sional structure of the fundamental persisted until after subharmonic growth was established. Three-dimensional distortions then appeared and coincided with the first post-equilibration alteration in fundamental mode energy. Three-dimensional mechanisms may thus play an important role in the breakdown of the fundamental mode equilibration but do not seem to be involved in the generation of the subharmonic modes.

Kelly also found that finite amplitude oscillations of the fundamental mode can interact with two latent disturbances, $\frac{1}{2}\beta$ and $\frac{3}{2}\beta$, so as to destabilize the $\frac{3}{2}$-harmonic mode. This agrees with figure 23, where contours of $\frac{3}{2}$-harmonic activity in regions IV–VI are confined to the areas where subharmonic and fundamental mode activity overlap.

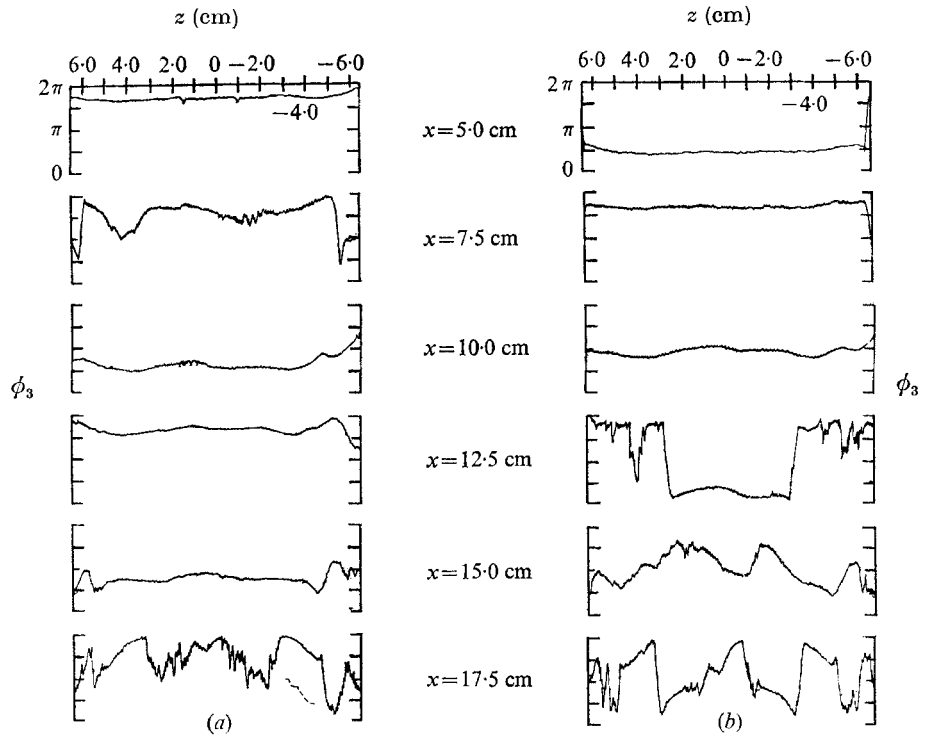

FIGURE 24. Spanwise variations in the phase of the $\beta = 0{\cdot}222$ disturbance. $\bar{u}_T = 245$ cm/s, $\bar{u}_B = 38$ cm/s, $R(x_0) = 180$. (*a*) $y = 0$. (*b*) $y = 0{\cdot}20$ cm.

Region V: *onset of three-dimensional activity and the termination of fundamental mode equilibration*

Fundamental mode equilibration terminates at about 3·5 wavelengths downstream and is accompanied by three-dimensional distortions of the mean flow and fluctuating components. The onset of spanwise activity coincides with a noticeable decay of fundamental mode energy along the $z = 0$ centre-plane. $u'_{\text{r.m.s.}}$ wave-front measurements indicate that this may be due to a spanwise redistribution of energy and not to a transfer of energy to other scales of motion.

All details of this region were not investigated but several features were evident. Initial spanwise variations in phase and $u'_{\text{r.m.s.}}$ were most pronounced in regions of large $\partial\bar{u}/\partial y$. Smoke trace measurements indicate the formation of a weak longitudinal vortex structure of ellipsoidal form with major axis along the spanwise co-ordinate. The initial spanwise scale of the vortices is of order λ, the fundamental mode wavelength. As three-dimensional activity increased, the spanwise scale decreased to roughly half to two-thirds of λ. At the same time, the vortices spread rapidly in the vertical direction.

The development of this vortex structure is in basic agreement with the Benney–Lin mechanism (1960), in which a two- and three-dimensional disturbance interact to reinforce spanwise distortions of the fundamental, and generate a longitudinal secondary vortex structure. They found that the theoretical

spanwise wavelength varied from that of the fundamental wavelength for weak three-dimensional effects to half that of the fundamental wavelength when strong three-dimensional effects dominate. A similar reduction in wavelength was noticed in the experiments as three-dimensional activity increased.

It is not clear whether the cross-stream boundaries exert spanwise constraints. At best, only two or three fundamental mode wavelengths can fit in the spanwise direction. This is not a sufficient degree of freedom to eliminate boundary effects. The influence of boundaries must be explored further to establish the representativeness of the three-dimensional mechanisms observed in this experiment.

Region VI: *final breakdown to turbulence*

Once a secondary vortex structure is established transition to turbulence occurs. The disturbance spectrum loses its discrete character and evolves into a continuous spectrum of intermittent disturbances. Phase measurements showed that the phase relationship with the upstream behaviour of the transition is lost. Spanwise phase profiles shown in figure 24 have pronounced distortions. Final transition is accompanied by the generation of weak secondary instabilities at the upper and lower edges of the shear layer, with dominent activity along the upper edge. Spectral measurements showed no evidence of high-frequency bursts. The intermittent secondary instabilities contained oscillations in the β–3β range. Although the frequencies of the secondary instabilities were not high in comparison to the frequency of the fundamental, their vertical scale was an order of magnitude smaller than the local scale of mean shear.

6. Conclusions

The experiments indicate that the instability of a free shear layer involves a series of nonlinear mechanisms. In the initial small-amplitude region, experiment is in agreement with spatial linear theory. Nonlinear effects become important at amplitudes of order 2×10^{-2} times the $\bar{u}_T$ velocity and indicate a strong restriction on the applicability of linear theory. At fundamental mode amplitudes greater than 2×10^{-2}, harmonic, subharmonic and $\frac{3}{2}$-harmonic modes are generated and grow at smaller exponential rates than those predicted by weak nonlinear theory. Although the experiments were run at relatively low Reynolds numbers, there is evidence that harmonic generation may involve nonlinear effects at the critical layer. The evidence of this lies solely in the observed harmonic growth rates, and the fact that $\Lambda = (\epsilon^{\frac{3}{2}}R)^{-1}$ approaches $O(1)$ as harmonic modes are generated. The applicability of the work of Benney & Bergeron and Robinson is not certain. The finite amplitude equilibration of the fundamental mode may involve three-dimensional effects but, in general, equilibration is described by the work of Landau (1944) and Stuart (1960). The equilibration process also seems to agree with Stuart's (1958) model, but Davey (1962) has pointed out some self-cancelling inconsistencies in Stuart's work and the significance of the result is not clear. The generation of subharmonic oscillations by finite amplitude oscillations of the fundamental is adequately described by Kelly's (1967) theory. However, as with the small-amplitude region instabilities, there is a need for

theoretical models which consider the spatial growth of disturbances. Three-dimensional effects seem to play an important role in the breakdown of fundamental mode equilibration. The onset of strong three-dimensional motions basically agrees with the Benney–Lin model. However, the small spanwise geometry of the test section may have influenced three-dimensional development. Transition to turbulence involves weak secondary instabilities but no evidence of turbulent bursts or sudden breakdown was observed.

The author would like to express his gratitude to Professor Erik Mollo-Christensen for his generous help and valuable suggestions and to Professor J. T. Stuart for his many comments and stimulating discussions. This research was conducted in the Department of Meteorology at the Massachusetts Institute of Technology under National Science Foundation grant G.A. 2339. The paper was prepared at Imperial College, under a grant from the Science Research Council of England.

REFERENCES

BENNEY, D. J. & BERGERON, R. F. 1969 A new class of nonlinear waves in parallel flows. *Studies in Appl. Math.* **48** (3), 181.

BENNEY, D. J. & LIN, C. C. 1960 On the secondary motion induced by oscillations in shear flow. *Phys. Fluids*, **3**, 656.

BETCHOV, R. & SZEWCZYK, A. 1963 Stability of a shear layer between parallel streams. *Phys. Fluids*, **6**, 1391.

BROWAND, F. K. 1966 An experimental investigation of the instability of an incompressible separated shear layer. *J. Fluid Mech.* **26**, 281.

DAVEY, A. 1962 The growth of Taylor vortices in flow between rotating cylinders. *J. Fluid Mech.* **14**, 336.

FREYMUTH, P. 1966 On transition in a separated laminar boundary layer. *J. Fluid Mech.* **25**, 683.

HOWARD, L. N. 1964 The number of unstable modes in hydrodynamic stability problems. *J. Mécanique*, **4**, 433.

KELLY, R. E. 1967 On the stability of an inviscid shear layer which is periodic in space and time. *J. Fluid Mech.* **27**, 657.

LANDAU, L. D. 1944 On the problem of turbulence. *C. R. (Dokl.) Acad. Sci. U.R.S.S.* **44**, 311.

LIU, J. T. C. 1969 Finite-amplitude instability of the compressible laminar wake. Weakly nonlinear theory. *Phys. Fluids*, **12**, 1763.

MATTINGLY, G. E. 1968 The stability of a two-dimensional incompressible wake. *Princeton University, Dept. of Aerospace and Mech. Sci. Rep.* no. 858.

MICHALKE, A. 1965 On spatially growing disturbances in an inviscid shear layer. *J. Fluid Mech.* **22**, 371.

MIKSAD, R. W. 1970 Experiments on free-shear-layer transitions. *M.I.T., Dept. Meteorology Rep.* 70-001 N.

RAETZ, G. S. 1959 *Northrop Rep.* NOR-59-383 (BLC-121).

SATO, H. 1956 Experimental investigation on the transition of laminar separated layer. *J. Phys. Soc. Japan*, **11**, 702.

SATO, H. 1959 Further investigation on the transition of two-dimensional separated layer at subsonic speeds. *J. Phys. Soc. Japan*, **14**, 1797.

SATO, H. 1960 Transition of a two-dimensional jet. *J. Fluid Mech.* **7**, 53.

SATO, H. 1971 An experimental study of nonlinear interaction of velocity fluctuations in the transition region of a two-dimensional wake. *J. Fluid Mech.* **44**, 741.

SATO, H. & KURIKI, K. 1961 The mechanism of transition in the wake of a thin flat plate placed parallel to a uniform stream. *J. Fluid Mech.* **11**, 321.

SATO, H. & OKADA, O. 1966 The stability and transition of an axisymmetric wake. *J. Fluid Mech.* **26**, 237.

STUART, J. T. 1958 On the nonlinear mechanics of hydrodynamic stability. *J. Fluid Mech.* **4**, 1.

STUART, J. T. 1960 On the nonlinear mechanics of wave disturbances in stable and unstable parallel flows. Part 1. The basic behaviour in plane Poiseuille flow. *J. Fluid Mech.* **9**, 353.

WATSON, J. 1960 On the nonlinear mechanics of wave disturbances in stable and unstable parallel flows. Part 2. *J. Fluid Mech.* **9**, 371.